Stability and Interactions of Transverse Field Structures in Optical Parametric Oscillators

Joel Nishimura

Department of Mathematics, University of Washington
email: joelnish@u.washington.edu, phone: (206) 384-8384

Abstract

A fourth-order order parameter equation of the Swift-Hohenberg type is derived for an optical parametric oscillator near its resonance detuning limit. The stability and behavior of solutions to this will be studied utilizing both numerical evolutions and linear stability calculations. The stability of 1D solutions in higher dimensions are reviewed as are previous 2D results. Additionally a localized solution (LS) in 2D with a broad basin of attraction and intricate LS-LS interaction is detailed and an analogous 3D solution is found.

Introduction

Optical parametric oscillators (OPOs) represent a classical application of nonlinear optics. In essence an OPO consists of a nonlinear crystal inside of an optical cavity (an optical cavity is a pair of mirrors opposing each other so that light is trapped between them) as depicted in figure 1. One of the defining characteristics of the OPO is its ability to take in a high power pump laser at frequency ω_p and generate light at two lower frequencies ω_s and ω_i where conservation of energy requires $\omega_p = \omega_i + \omega_s$. These three fields are called the pump, signal and idler fields respectively. Traditionally the optical parametric oscillator has been used as a source of tunable coherent radiation and high energy pulses. However, as in many nonlinear devices it is possible to balance the cavity diffraction with material nonlinearity in order to create a localized, steady-state solution. The creation of such localized solutions (LS) is of critical importance not only for traditional optical applications, such as communication, but also for creating "bits" for all optical computing machines.

Since the goal of the OPO is to create the signal field from the pump field the most important consideration is the behavior near the resonance detuning limit, when the constant solution zero is no longer stable the signal field. Indeed much of the previous work on the OPO has concentrated on this point. While there are many possible order parameter equations (OPE) that can be derived for the OPO near the resonance detuning limit the most general is of a Swift-Hohenberg type with quintic nonlinearity and additional cubic terms derived in 1D by [1]. It should be noted that much work has been done on a parameter regime where the dynamics are governed by an equation without many of the cubic terms, where the quintessential Swift-Hohenberg behaviors of stripes and hexagonal patterns are present [3]. The addition of these cubic terms allows for analytic 1D solutions found in [1]. Furthermore [2] details the behavior of some solutions found in 2D.

If these LS are to be used though, it is critical that not only their stability be considered but also their interaction with other structures. This however is an especially hard question to ask analytically, though it is readily approachable from a numerical perspective. Using the exponential time-differencing scheme outlined in [4] we have found a family of localized and stable steady-state solutions. Furthermore, using the Floquet-Fourier-Hill method outlined in [8] we analyze the linear stability of these solutions and also review the stability of the

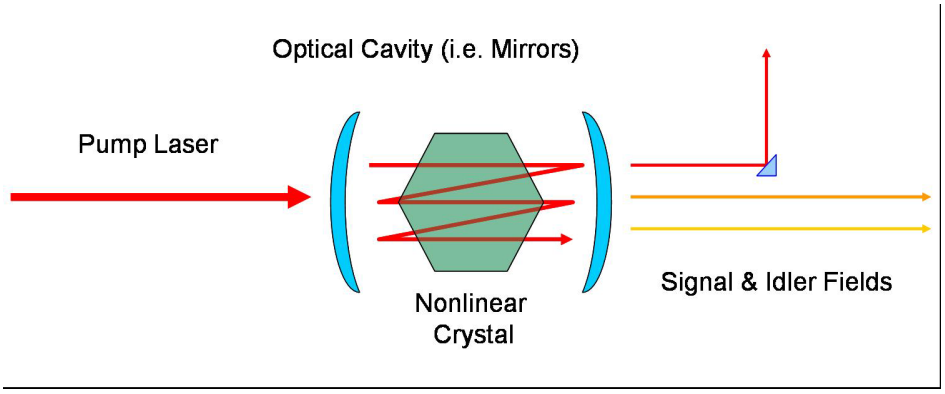

Figure 1: Shown above is a slimple depiction of an idealized optical parametric oscillator. A single pump laser is shown into the optical cavity, where it continuously traverses the inside of a nonlinear crystal. Coupling creates two additional fields inside the crystal, namely the signal and idler fields. Eventually the signal field is diverted to be used in some application.

analytic 1D solutions in higher dimensions. Additionally we look at the type of interactions allowed between LS and how these interactions change with the parameters. Of particular note, it is found that under some parameter regimes solitons of opposite sign attract and orient themselves into lines or polygons. There also exist parameter regimes in which the LS have almost no interactions with each other, even when spatially close. We also look at a variety of solutions in 3D. Due to the computing difficulty associated with increasing dimensions the Floquet-Fourier Hill method is unavailable to us in 3D. However, direct numerical integration reveals that while many of the two dimensional solutions are unstable when put into 3D, they have natural 3D correlates that behave similarly to their 2D versions.

1 The Equations

The electromagnetic wave structures inside of an OPO are governed by Maxwell's equations. From Maxwell's equations and the knowledge of the nonlinear crystal it is possible to derive the system of three coupled partial differential equations [5] [6]:

$$u_t = \frac{i}{2}\bigtriangledown^2 u + wv^* - (1+i\Delta_1)u \tag{1a}$$

$$v_t = \frac{i}{2}\bigtriangledown^2 v + wu^* - (1+i\Delta_2)v \tag{1b}$$

$$w_t = \frac{i\rho}{2}\bigtriangledown^2 w - uv - (\alpha+i\Delta_3)w + S \tag{1c}$$

where, u and v are the signal and idler fields respectively, * denotes the complex conjugate, $\bigtriangledown^2$ is the Laplacian in terms of spatial coordinates (x, y, z) and w is the pump field. α, ρ and the Δ's are parameters of the system and S is the strength of the pumping field. In the

degenerate case the u and v field are at the same frequency and the three coupled equations become a pair of coupled equations in a natural way.

1.1 A Simple Solution and Linear Stability

Notice (1) has a uniform solution for,

$$\begin{aligned} u &= 0 && \text{(2a)} \\ v &= 0 && \text{(2b)} \\ w &= \frac{S}{\alpha + i\Delta_3} && \text{(2c)} \end{aligned}$$

which becomes unstable at a critical value of the pumping field S_c. We perturb around this critical value of S_c with:

$$\begin{aligned} u &= 0 + \tilde{u} && \text{(3a)} \\ u &= 0 + \tilde{v} && \text{(3b)} \\ w &= \frac{S_c}{\alpha + i\Delta_3} + \tilde{w} && \text{(3c)} \end{aligned}$$

where,

$$\begin{aligned} \tilde{u} &= \Sigma e^{\lambda_1 t}\cos(k_1 x) && \text{(4a)} \\ \tilde{v} &= \Sigma e^{\lambda_2 t}\cos(k_2 x) && \text{(4b)} \\ \tilde{w} &= \Sigma e^{\lambda_3 t}\cos(k_3 x) && \text{(4c)} \end{aligned}$$

Linearizing about this solution of (1) and using the fact that $k = 0$ is the most unstable wave number leads to:

$$\begin{aligned} \lambda_1 u &= \frac{S_c}{\alpha + i\Delta_3} v - (a + i\Delta_1)u && \text{(5a)} \\ \lambda_2 v &= \frac{S_c}{\alpha + i\Delta_3} u - (a + i\Delta_2)v && \text{(5b)} \\ \lambda_3 w &= -(\alpha + i\Delta_3)w && \text{(5c)} \end{aligned}$$

Notice then that the stability of the w field is independent of both the u and v fields. Furthermore both the real and imaginary parts of λ_3 are negative for positive α and Δ_3. Thus the stability of the system is determined by the $4 - by - 4$ system A consisting of the real and imaginary parts of u and v, giving:

$$A = \begin{bmatrix} -1 & d1 & \frac{Sc\,a}{a^2+d3^2} & -\frac{Sc\,d3}{a^2+d3^2} \\ -d1 & -1 & -\frac{Sc\,d3}{a^2+d3^2} & -\frac{Sc\,a}{a^2+d3^2} \\ \frac{Sc\,a}{a^2+d3^2} & -\frac{Sc\,d3}{a^2+d3^2} & -1 & d2 \\ -\frac{Sc\,d3}{a^2+d3^2} & -\frac{Sc\,a}{a^2+d3^2} & -d2 & -1 \end{bmatrix}.$$

The eigenvalues of this system depend only on the modulus squared of S_c. Additionally the largest real eigenvalue of this system becomes zero when:

$$|S_c| = |(\alpha + i\Delta_3)\sqrt{(1 + i\Delta_1)(1 + i\Delta_2)}|. \tag{6}$$

For S with modulus smaller than this all the eigenvalues have negative real part, which implies that the steady state, uniform solution is stable. However, for S larger than this A has an eigenvalue with positive real part and thus the solution is unstable. This implies that the solution has a bifurcation point at $S = S_c$. This leads naturally to a perturbation expansion.

1.2 Derivation of the Order Parameter Equation

The general point of a perturbation expansion is to capture the behavior of the system about a single point of interest, in this case the point where S drives the OPO off of the trivial solution. However, in order to capture the preferred behavior it is sometimes necessary to rescale the parameters, the dimensions or boths. This leads to a large number of possible OPE, and indeed there are numerous different perturbation expansions that have been performed on the OPO. Many previous derivations of various OPE have focused on isolating Swift-Hohenberg terms, as these already somewhat well understood [3]. However, as in [1], [2] and [7], additional terms are retained both because they allow some analytic constructions and to keep the equation more physically relevant. The manner of this derivation owes heavily to the method utilized on the degenerate OPO used in [1], though it has been extended to include the non degenerate case.

With the value of critical value of the pump determined we now perturb about the uniform steady solution with:

$$u = 0 + \epsilon u_1 + \epsilon^2 u_2 + ... \tag{7a}$$
$$v = 0 + \epsilon v_1 + \epsilon^2 v_2 + ... \tag{7b}$$
$$w = \frac{S}{\alpha + i\Delta_3} + \epsilon w_1 + \epsilon^2 w_2 + ... \tag{7c}$$

where,

$$S = S_c + \epsilon^2 C_1 + \epsilon^4 C_2 + ... \tag{8}$$

Additionally we change the scales of time and space so that, $X = \epsilon x$, $Y = \epsilon y$, $Z = \epsilon z$ and $\tau = \epsilon^4 t$. We also impose resonance restrictions on the detuning,$\Delta_1 = \Delta_2 = \epsilon^2\kappa$ and $\alpha - \Delta_1\Delta_3 = \epsilon^2\beta$ (where $\alpha \sim O(\epsilon^2)$ and $\Delta_3 \sim O(1)$). These changes of variables and expansions of u, v, and w are plugged into our order parameter equation (14) to give a long expression with different powers of ϵ. We collect terms according to their powers of ϵ. At $O(1)$ we have trivially satisfied equations. At $O(\epsilon)$ we find that:

$$I) \quad 0 = -(1 + i\Delta_1)U_1 + \frac{S_c}{\alpha + i\Delta_3}V_1^* \tag{9a}$$

$$II) \quad 0 = \quad -(1+i\Delta_1)V_1 + \frac{S_c}{\alpha+i\Delta_3}U_1^* \tag{9b}$$

$$III) \quad 0 = \quad -W_1(\alpha+i\Delta_3) \tag{9c}$$

Notice that this gives that $W_1 = 0$, U_1 is equal to some constant times V_1^*, and furthermore that $|U_1| = |V_1|$. (The condition that $V_1 = U_1^*$ has a cousin in the degenerate case, namely $U_{1,degen} = U_{1,degen}^*$, which gives that U_1 is real valued. That U_1 and V_1 are not forced to be real at this point will result in the one difference between the degenerate OPE and the non-degenerate OPE, that the non-degenerate case is complex valued.) Also at $O(\epsilon)$ we see the consistent linear operator that will appear in each order of the expansion from this point forward. We define,

$$L_{1,2,3}(U_n, V_n, W_n) = \left\{ \begin{array}{c} \frac{S_c}{\alpha+i\Delta_3}V_n^* - (1+i\Delta_1)U_n \\ \frac{S_c}{\alpha+i\Delta_3}U_n^* - (1+i\Delta_2)V_n \\ -W_n(\alpha+i\Delta_3) \end{array} \right\}.$$

Since each further order of the expansion will be of the form:

$$L_{1,2,3}(U_n, V_n, W_n) = R_{1,2,3}(U_1, ..., U_{n-1}, V_1, ..., V_{n-1}, W_1, ..., W_{n-1}) + O(\epsilon^2), \tag{10}$$

it turns out that each W_k, $k \leq n$ can be written as $R_3(U_1, ..., U_{n-1}, V_1, ..., V_{n-1})$. In other words W is trivially solvable and other instances of W can be substituted out. This allows that $L_1 = R_1$ can be manipulated to give U_n in terms of $V_1, ..., V_{n-1}$ to within $O(\epsilon^2$, which provides a way to decouple all the fields. It is thus not a surprise that the equations given by the expansion will end up being extremely similar to the degenerate case. However, before we continue with the expansion we must first derive some solvability conditions.

Since $L_{1,2}$ is linear, it is possible to write it as a matrix operation, . In this case we have that:

$$\left[\begin{array}{c} Re(L_1) \\ Im(L_1) \\ Re(L_2) \\ Im(L_2) \end{array} \right] = \left[\begin{array}{cccc} -1 & d1 & \frac{Sc\,a}{a^2+d3^2} & -\frac{Sc\,d3}{a^2+d3^2} \\ -d1 & -1 & -\frac{Sc\,d3}{a^2+d3^2} & -\frac{Sc\,a}{a^2+d3^2} \\ \frac{Sc\,a}{a^2+d3^2} & -\frac{Sc\,d3}{a^2+d3^2} & -1 & d2 \\ -\frac{Sc\,d3}{a^2+d3^2} & -\frac{Sc\,a}{a^2+d3^2} & -d2 & -1 \end{array} \right] \left[\begin{array}{c} Re(U) \\ Im(U) \\ Re(V) \\ Im(V) \end{array} \right] = \left[\begin{array}{c} Re(R_1) \\ Im(R_1) \\ Re(R_2) \\ Im(R_2) \end{array} \right].$$

Notice that this system is not necessarily solvable for U and V. In order to enforce that the system is solvable we require that R_1 and R_2 are orthogonal to the null space of the adjoint operator. Using the fact that $\Delta_1 = \Delta_2$ we find that to be orthogonal to the eigenvectors associated with the zero eigenvalues requires that R_1 and R_2 satisfy:

$$(1-i\Delta_1)R_1 + \frac{S_c}{\alpha+i\Delta_3}R_2^* = 0 \tag{11a}$$

$$(1-i\Delta_1)R_2 + \frac{S_c}{\alpha+i\Delta_3}R_1^* = 0. \tag{11b}$$

These solvability conditions will later be imposed on results that we obtain using recursion, and will be responsible for generating the fourth order terms among others.

With a clear set of solvability conditions laid out we return to our expansion, following the same method of proof as [1] and [2]. If one turns their attention only to U_1, V_1 and W_1 then it possible to write the perturbation expansion as:

$$I) \quad \epsilon^5 U_\tau = \epsilon^3 \frac{i}{2} \bigtriangledown^2 U + \epsilon^3 W V^* + \epsilon^3 \frac{CV^*}{(\alpha + i\Delta_3)} - \epsilon(1 + i\Delta_1)U + \epsilon \frac{S_c V^*}{(\alpha + i\Delta_3)} \quad (12a)$$

$$II) \quad \epsilon^5 V_\tau = \epsilon^3 \frac{i}{2} \bigtriangledown^2 V + \epsilon^3 W U^* + \epsilon^3 \frac{CU^*}{(\alpha + i\Delta_3)} - \epsilon(1 + i\Delta_1)V + \epsilon \frac{S_c U^*}{(\alpha + i\Delta_3)} \quad (12b)$$

$$III) \quad \epsilon^6 W_\tau = \epsilon^4 \frac{i\rho}{2} \bigtriangledown^2 W + \epsilon^2 UV + \epsilon^2(\alpha + i\Delta_3)W \quad (12c)$$

Since I and II are symmetric up to a substitution of U for V we will work only with I assuming that analogous results hold true for II. Solving for W from III gives us:

$$W = -\frac{UV}{\alpha + i\Delta_3} + \epsilon^2 \frac{i\rho \bigtriangledown^2 (W)}{2(\alpha + i\Delta_3)} + O(\epsilon^4) \quad (13)$$

However, since $W = -UV + O(\epsilon^2)$ we can use this recursively to replace $\bigtriangledown^2(W)$, with $\bigtriangledown^2(-UV)$. This then gives us an expression for W which we can plug into I, giving us:

$$\epsilon^4 U_\tau = -(1 + i\Delta_1)U + \frac{S_c V^*}{(\alpha + i\Delta_3)} + \epsilon^2(\frac{i}{2} \bigtriangledown^2 U - \frac{UVV^*}{\alpha + i\Delta_3} + \frac{CV^*}{(\alpha + i\Delta_3)}) + \epsilon^4 \frac{i\rho \bigtriangledown^2 (UV)}{2(\alpha + i\Delta_3)} V^* + O(\epsilon^5)$$

which can be rewritten as:

$$\begin{aligned} R_1 = (1 + \Delta_1)(U - V^*) = \quad & +\epsilon^2(\tfrac{i}{2} \bigtriangledown^2 U - \tfrac{UVV^*}{\alpha + i\Delta_3} + \tfrac{CV^*}{(\alpha + i\Delta_3)}) + ... \\ & ... + \epsilon^4(\tfrac{i\rho \bigtriangledown^2 (UV)}{2(\alpha + i\Delta_3)} V^* - U_\tau) + O(\epsilon^5) \end{aligned}$$

or rewritten instead to give an expression for $V^* = U - \frac{R_1}{(1+\Delta_1)}$. In the same way that recursion was used to find that W solely in terms of U and V we can use recursion with this expression for V^* to find an expression for V^* solely in terms of U and $O(\epsilon^4)$ terms. Similarly, we get an expression for U^* and R_2 by symmetry which also gives us $|U| = |V|$. Now that we have an expression for R_1 and R_2 it is possible to substitute them into our solvability expressions (11). At this point we need only one of these expressions, let it be (11a), giving:

$$\begin{aligned} 0 = \quad & (1 - i\Delta_1)(+\epsilon^2(\tfrac{i}{2} \bigtriangledown^2 U - \tfrac{UVV^*}{\alpha + i\Delta_3} + \tfrac{CV^*}{(\alpha + i\Delta_3)}) + \epsilon^4(\tfrac{i\rho \bigtriangledown^2 (|U|^2)}{2(\alpha + i\Delta_3)} V^* - U_\tau)) + ... \\ & ...(1 + i\Delta_1)(+\epsilon^2(\tfrac{i}{2} \bigtriangledown^2 V^* - \tfrac{V^*|U|^2}{\alpha + i\Delta_3} + \tfrac{CU}{(\alpha + i\Delta_3)}) + \epsilon^4(\tfrac{i\rho \bigtriangledown^2 (|U|^2)}{2(\alpha + i\Delta_3)} U - V_\tau^*) + O(\epsilon^5)) \end{aligned}$$

Since this contains only U and V^* terms, and we have an expression for V^* in terms of U terms then this equation can be decoupled to include only U and $|U|$ terms. At this point we can Collect terms and use our detuning assumptions, that $\Delta_1 = \Delta_2 = \epsilon^2 \kappa$ and $\alpha - \Delta_1 \Delta_3 = \epsilon^2 \beta$. Extensive simplification and discarding $O(\epsilon^2)$ terms leads to our OPE:

$$u_\tau + \frac{1}{4}(\bigtriangledown^2 - \omega)^2 u - \gamma u - \sigma u^3 + u^5 + 3\delta u(\bigtriangledown u \cdot \bigtriangledown u) + 2\delta u^2 \bigtriangledown^2 u = 0 \tag{14}$$

where the signal field u is the first order perturbation, U. As in [2] $x = X/\sqrt{|\Delta_3|}$, $y = Y/\sqrt{|\Delta_3|}$, $z = Z/\sqrt{|\Delta_3|}$ and $t = \tau/(2\sqrt{|\Delta_3|})$. Similarly we impose consistent notation with [2], letting $\sigma = -2\beta$, $\omega = |\Delta_3|\Delta_1/(2\epsilon^2)$, $\gamma = 2\beta C + C^2 + \omega^2/4$, and $\delta = \pm 1$, the sign of Δ_3. However, unlike the degenerate case u is a complex value. Notice that this equation has Swift-Hohenberg terms $(\bigtriangledown^2 - \omega)^2 u$. The additional cubic terms at the end of the equation though are not common in most Swift-Hohenberg type equations, but are important, because as demonstrated in [1] allow for the construction of analytic 1D solutions. Indeed, these cubic terms, and their associated derivative terms, combined with the quintic term allow one to add out the fourth derivative of a hyperbolic secant, per say. Also, since every term is of an odd power of u then the negative of a solution is a solution as well. Although we have taken the effort to derive the OPE for the nondegenerate case there is enough interesting behavior solely in the degenerate to restricting our attention to the degenerate case.

2 Calculating Linear Stability

Questions of stability have always been of critical importance in the consideration of solutions to differential equations. For nonlinear PDE's the question of stability can in part be addressed by linear stability, and the corresponding eigenvalue spectrum of the linearized operator. Ideally such calculations are done analytically based off of a closed form solution. Even without analytic solutions though it is still possible to calculate eigenvalues and their associated eigenvectors or eigenfunctions numerically. The most prevalent method to perform such calculations based off of numerical data is a method based around finite difference techniques. Another method that can be used to calculate the eigenvalue spectrum of a linear operator is the Floquet-Fourier Hill method, which transforms the linear operator into the spectral domain, providing both accuracy and computational bonuses.

2.1 An Eigenvalue Problem

Given our nonlinear PDE (14) we linearize by assuming a solution of the form:

$$u = u_0 + \hat{u}e^{\lambda t} \tag{15}$$

for an exact solution on an infinite domain, u_0 and small perturbation $\hat{u}$. After using the fact that u_0 is an exact solution and collecting only terms linear in $\hat{u}$ we are left with $\lambda\hat{u} = L(\hat{u})$ where the linearized operator L is:

$$L(\hat{u}) = -\frac{1}{4}(\bigtriangledown^2 - \omega)^2\hat{u} + \gamma u + 3\sigma u_0^2\hat{u} - 5u_0^4\hat{u} - 3\delta\hat{u}(\bigtriangledown u_0 \cdot \bigtriangledown u_0) - ...$$
$$...6\delta u_0(\bigtriangledown\hat{u} \cdot \bigtriangledown u_0) - 2\delta u_0^2 \bigtriangledown^2 \hat{u} - 4\delta u_0\hat{u} \bigtriangledown^2 u_0$$

Since $\lambda\hat{u} = L(\hat{u})$ then knowing the eigenvalues of the linear operator will give us the linear stability of the system. With this setup we can now turn towards the Floquet-Fourier Hill Method to calculate these eigenvalues for solutions existing on large periodic domains.

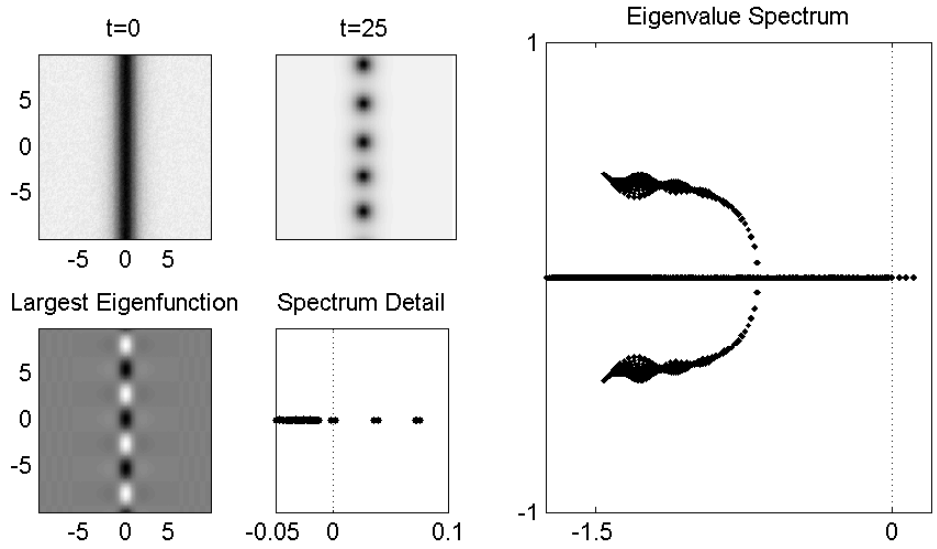

Figure 2: The evolution of a *sech* with noise from $t = 0$ (top left) to $t = 25$ (top center right) displays the realization of the largest eigenfunction (bottom left). Shown in the far right plot is the eigenvalue spectrum of the linearized operator about the sech solution; the eigenvalues with positive real part are detailed in the bottom right plot. Thus, while stable in 1D this hyperbolic secant is unstable in 2D. Notice that the instability of this solution leads to solutions that are themselves localized.

2.2 The Fast-Fourier Hill Method

A complete description of this method can be found in [8] and it should be noted that the recent SpetrUW program implements this method (though I wrote my own version for this). The core idea behind the Floquet-Fourier Hill method is to transform the linear operator into the Fourier domain, collect the terms corresponding to the same exponential functions and then arrange those terms into the proper matrix. In order to then compute the eigenvalues of that matrix it must necessarily be truncated, which is the only step that limits accuracy. Notice that this is an extremely general procedure that requires little to no tailoring between different problems and can be done using numerical data.

3 1D Solutions Revisited

One of the critical differences between the general Swift-Hohenberg equations and our OPE, (14), is that the combination of the quintic nonlinearity and fourth order diffusion with some of the cubic terms allows for exact 1D solutions as in [1]. In particular there exists exact solutions taking the forms of tanh, sech, cn, sn and dn along with constant solutions. The stability of these solutions was explored in [1] with the conclusion that in 1D there exist stable regimes for all of these solutions. The stability of these solutions in higher dimensions is of critical practical importance though.

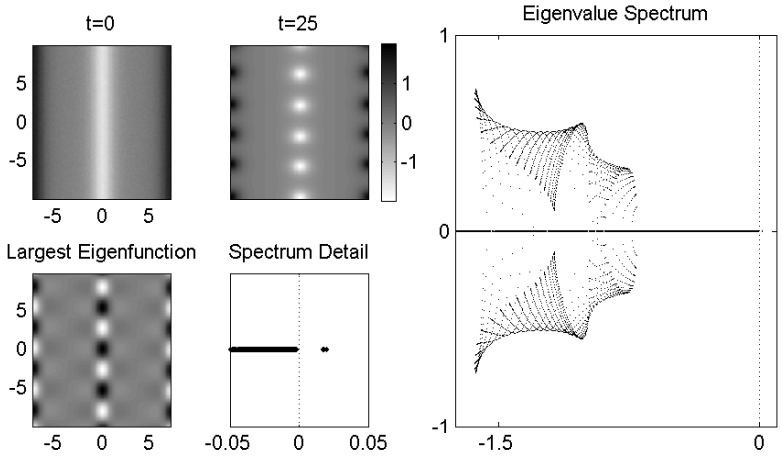

Figure 3: Displayed in this graph are the evolution, eigenvalue spectrum and largest eigenfunction of the elliptic function $A\text{cn}(Bx, k)$ for $A = 1.2987$, $B = 1.3$, $k = .999$, $\gamma = .1167$, and $\omega = \sigma = 1$. Much like the sech solution in figure 2, this solution's evolution (top left and right) realized the instability predicted by the largest eigenfunction in the bottom left plot. Also notice that the this instability is not part of the essential spectrum, as shown in the detail of the spectrum (bottom right). This is a prime example of how the stable 1D cn solutions go unstable in 2D.

The hyperbolic secant given by $u = \eta\text{sech}(\eta x)$, $\eta^2 = 1 \pm 2\sqrt{\gamma}$ is stable solution of the 1D version of (14) for $\gamma < 1/4$ provided that $\delta = 1$ and $\omega = \sigma$ [1]. As seen in figure 2 the embedding of this solution into 2D does not preserve linear stablity. Interestingly though, the instability of the 1D sech leads to localized 2D solutions, that when isolated are steady-state stable solutions. Similarly both cn and dn solutions demonstrate instabilities that lead to a set of localized 2D solutions of their own, as seen in figures 3 and 4. In particular the behavior of these 2D instabilities will be addressed later in their own section.

The hyperbolic tangent given by $u = \eta\tanh(\eta x)$, $\eta^2 = 1 \pm \sqrt{\gamma}$ is a stable solution of the 1D version of (14) for a range of γ values providing that $\delta = -1$ and $\omega = -\sigma = -2$ [1]. Similarly the sn branch of solutions also remained stable when embedded into 2D. A further examination of solutions with large plateaus and sharp transitions is contained in the next section.

4 2D Structures

Much work has already been done on the OPE given in equation (14) in [2], where the stability of planewaves was detailed in complete generality as well as details of the behavior of periodic solutions and quasi-stable localized solutions. A prime example of a quasi-stable solution is the double sech, $A\text{sech}(BX)\text{sech}(BY)$. Figure 5 displays the slowgrowth of this structure, which remains almost, seemingly, steady-state until it begins to plateau. Figure 6 and figure 7 displays the interaction of the plateau structures, where the curvature of the

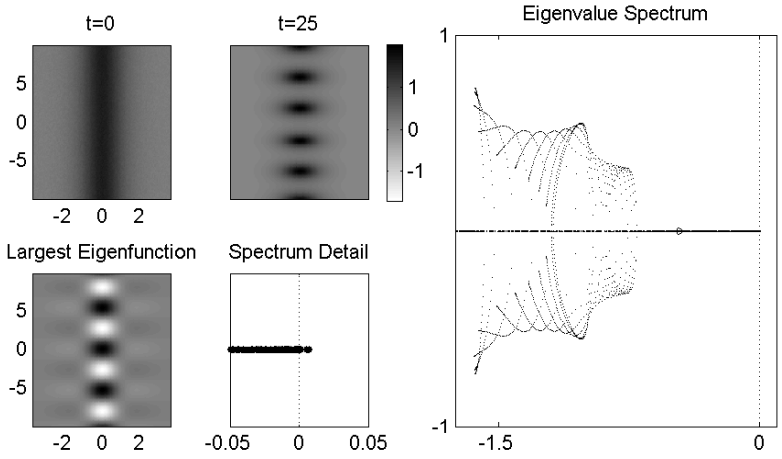

Figure 4: Displayed in this graph are the evolution, eigenvalue spectrum and largest eigenfunction of the elliptic function $A\text{dn}(Bx, k)$ for $A = 1.3$, $B = 1.3$, $k = .999$, $\gamma = .1167$, and $\omega = \sigma = 1$. Much like the sech and cn solution in figures 2 and **??**, this solution's evolution (top left and right) realized the instability predicted by the largest eigenfunction in the bottom left plot. Also notice that this instability is not part of the essential spectrum, as shown in the detail of the spectrum (bottom right). This is a prime example of how the stable 1D dn solutions go unstable in 2D.

boundary is minimized.

4.1 A Steady-State Localized Solution

Figure 8 shows the evolution of a stable soliton from a simple Gaussian with added noise and parameters $\gamma = .03$, $\omega = .4$, $\delta = 1$ and $\sigma = .5$. It should be noted that this structure can be generated from initial conditions far more general than a Gaussian. Indeed solutions such as the one in figure 9 can be generated from noise off of a plane wave, though it is unlikely to create a single LS. Furthermore the spectrum of the linearized operator contains only negative, real eigenvalues as seen in figure 8. Of particular interest is the tail of the LS, as the tail determines interactions with other structures. This solution is radially symmetric with a cross section that varies with parameters as seen in figure 9.

Since these solutions are radially symmetric it makes sense to transform (14) to radial coordinates giving:

$$u_t + \frac{1}{4}(u_rrrr + \frac{2}{r}u_rrr - \frac{1}{r^2}u_rr + \frac{1}{r^3}u_r - 2\omega(u_rr + \frac{1}{r}u_r) + \omega^2 u) - ...$$
$$...\gamma u - \sigma u^3 + u^5 + 3\delta u(u_r)^2 + 2\delta u^2(u_rr + \frac{1}{r}u_r) = 0$$

which while has many fewer dimensions has an unpleasant singularity at $r = 0$ that prevents direct numerical evolution. However, this equation can give us some insight into

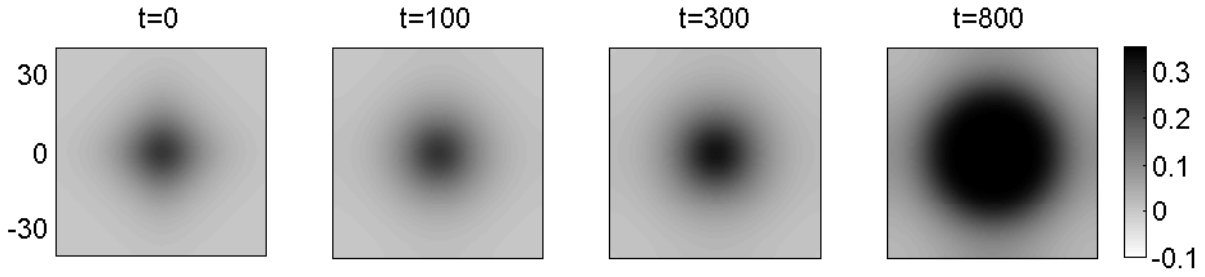

Figure 5: The evolution of a double sech in time for $\gamma = .1$, $\omega = .46$, and $\sigma = .466$. As seen above, the growth of this structure is extremely slow for the first few hundreds time units. However, eventually the slow radial expansion of the plateau will cover the domain.

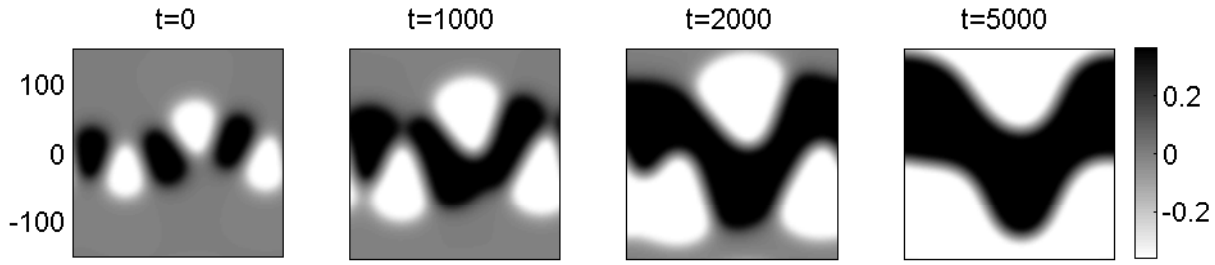

Figure 6: Using the same parameter regime as in figure 5 the evolution of several double sech structures, of alternating sign is explored. Notice that the transition from the positive to negative amplitude regions preserves both the positive and negative structures, though the overall behavior is determined by the curvature of the boundaries. Though not seen in this time series, the eventual stable behavior of this system is a banded pattern.

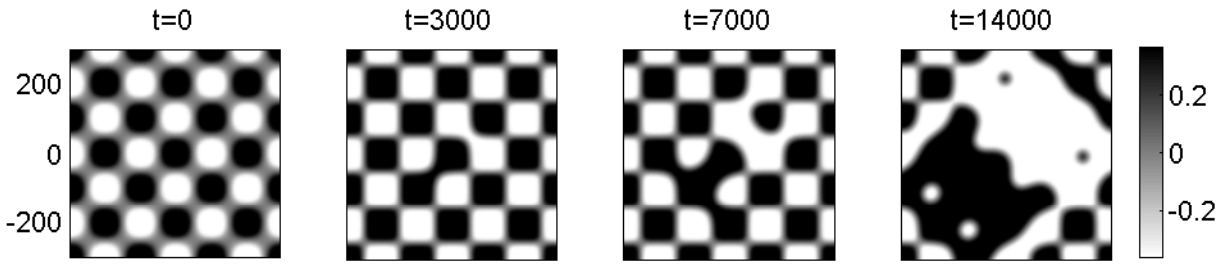

Figure 7: With the same parameters as figures 5 and 6 this shows the evolution of a grid of plateau regions. The only noise seeded in this evolution is the slight dislocation of the cental block. This small change though is enough to drive the system to become a simple plane wave of negative amplitude. The minimization of the boundary curvature leads these solutions to be able to create stable 1D patterns, but not stable nontrivial 2D solutions.

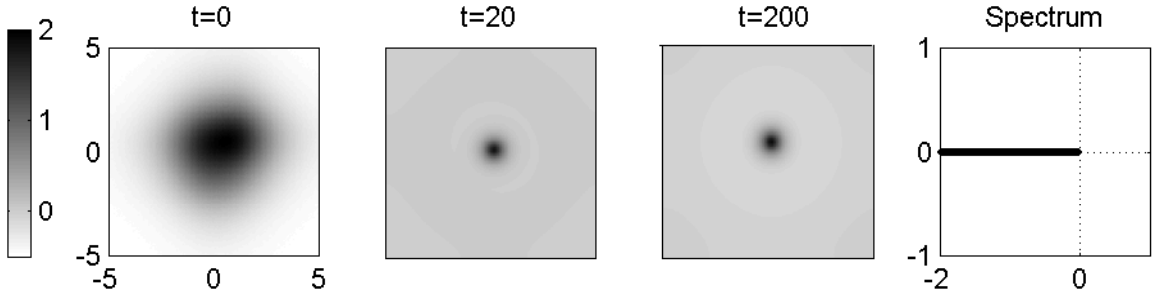

Figure 8: This is the evolution of a stable LS from a non distinct lump under the parameter regime $\gamma = .03$, $\omega = .4$ and $\sigma = .5$. The eigenvalue spectrum (right) explicitly shows that the LS is linearly stable. Of particular note is that this LS has a positive maximum and tails with negative values, which will allow for interesting LS-LS interactions.

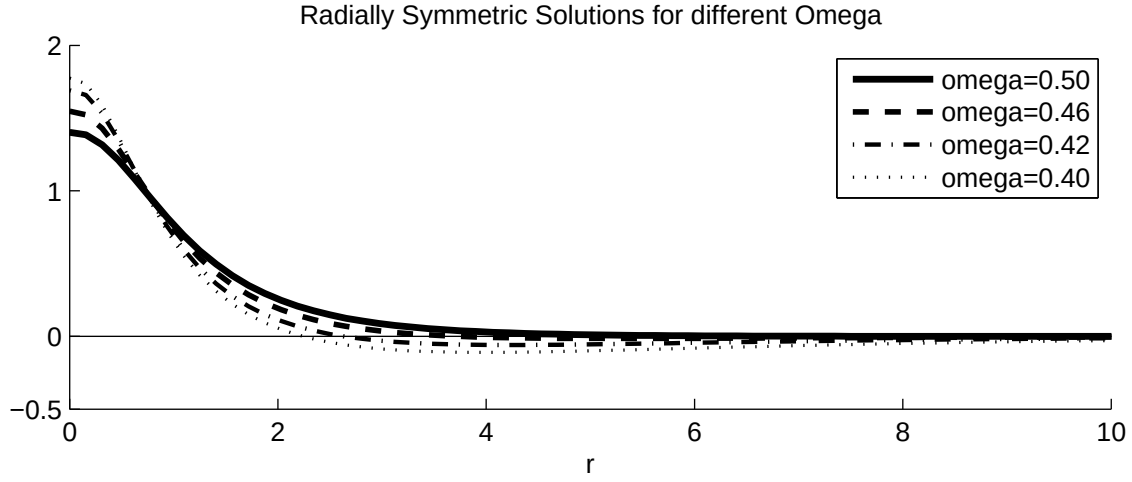

Figure 9: Displayed above is radial components of the LS for a variety of ω values with $\gamma = .03$ and $\sigma = .5$. Notice that at $\omega = .5$ the tail is monotonically decreasing, while at $\omega = .4$ the tail has a local minimum. The tail structure is especially important as it will determine the possible LS-LS interactions.

the structures of the LS tails.

4.2 LS Tails and LS-LS Interactions

To investigate the structure of the tails we use boundary layer theory. Looking at long length scales, $\tau = \frac{r}{\epsilon}$, steady state and low amplitude solutions, $u_t = 0$ and $u = \epsilon\hat{u}$ and requiring that $c = \epsilon(1/4)(\omega^2 - \gamma)$ we find that the tails are governed by:

$$-\frac{1}{2}\omega(u_{\rho\rho} + \frac{1}{\rho}u_\rho) + cu = 0 \tag{16}$$

the exact implications of this are still being worked out. In particular we are hoping to use power series to be able to better describe the behavior of the LS tail structure. Indeed as the tail changes shape so does the extent that solutions interact with each other. There are parameter regimes for which everything from relatively minimal to vital interactions occur between LS.

4.2.1 Monotonic Tails

In some regimes, such as $\omega = \sigma = .5$ and $\gamma = .03$, in which the LS has a monotonically decreasing tail LS-LS interaction is straightforward. As seen in figure 10 LS-LS interaction is simply attraction leading to merging. Similarly, LS of opposite sign repel. Since LS are by themselves stable, and LS-LS interactions can't create more LS, this regime often evolves to a set of distant LS, which interact at negligible long time periods.

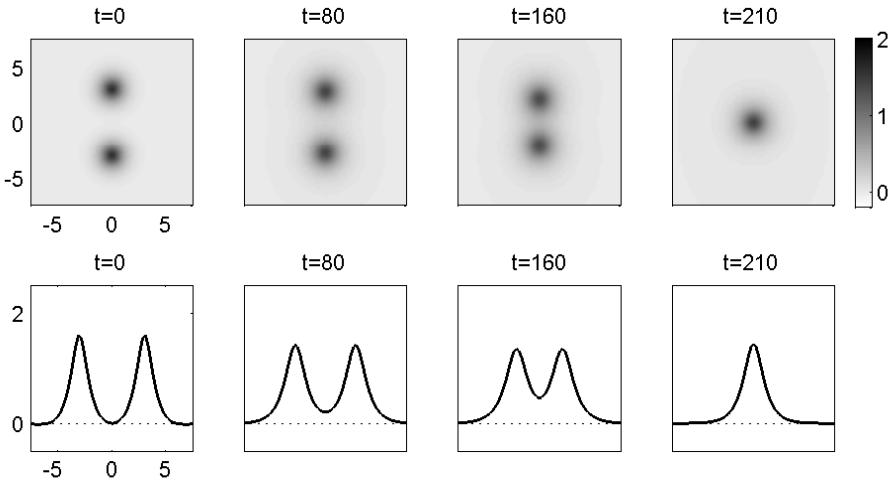

Figure 10: Shown above is the evolution of two separate LS in the parameter regime $\gamma = .03$, $\sigma = .5$ and $\omega = .5$, a regime in which LS have monotonic tails. A slice of the data for $y = 0$ is shown in the bottom. The speed of the initial attraction is minimal, as it must be conducted by the exponentially decreasing tail structures, while the eventual collapse occurs on a much faster time scale.

4.2.2 Non Monotonic Tails

In regimes such as $\omega = .4$, $\sigma = .5$ and $\gamma = .03$ the tails of the LS have a local extremum. Not only does this allow the solution to have a large shelf, it drastically changes the types of interactions possible between LS, allowing for self organizing structures.

The most basic type of interaction in this regime can be seen in figure 11, in which two LS with opposite signs attract and stabilize each other. This is unlike the interaction seen between two LS of the same sign, in which the two LS collapse into each other, as in figure 13, or spontaneously create a LS with the opposite sign, as in figure 12. Indeed, these three types of interactions between pairs of LS explain much of the possible interactions.

Figure 14 displays the evolution of a ring composed of six solitons, alternating in sign, from six double hyperbolic secants ($u = A\text{sech}(Bx)\text{sech}(By)$) and noise. This arrangement of LS is also stable under small dislocations of the individual LS as follows from the linear spectrum calculation. Though, the evolution seen in figure 14 further suggests that in actuality the ring is stable for not insignificant LS dislocation. Similarly figure 15 displays a ring composed with twelve LS. In general a stable ring can be formed out of any even number of LS including lines that wrap around the periodic boundary. Line segments have also been observed to be stable.

The combination of all these behaviors can be seen in figure 16, which displays the evolution off of a plane wave with noise. Notice that this evolution has several stages. In the first stage the noise on the plane wave generates an almost hexagonal pattern of solutions all with positive extrema, since the plane had a positive amplitude. The imperfect positioning, though, leads to the creation to the negative LS structures, which multiply. Eventually the

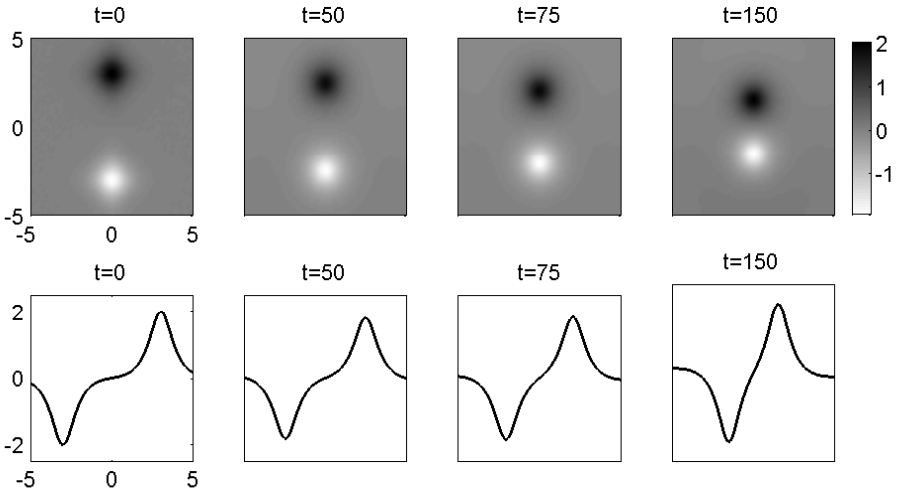

Figure 11: Shown above is the evolution of two LS of opposite sign in the parameter regime $\gamma = .03$, $\sigma = .5$ and $\omega = .4$, notable for having LS with non monotonic tails. Notice that between these LS of opposite sign there is a preferred separation. Separation greater than this leads to attraction, smaller, to repulsion.

LS organize themselves into patterns of lines, rings and grids. The creation of negative LS from a field of positive LS is a result of the negative section of the LS tail in this regime, and is not common in regimes where the tail is strictly positive.

4.3 Hexagonal Solutions

Also present are the hexagonal patterns Swift-Hohenberg equations are famous for. Indeed in some parameter regimes where the LS becomes unstable, it does so in a way that spontaneously generates LS type structures. Figure 17 shows LS instability and the generation of a field of structures that tend towards a hexagonal structure. Notice again that this evolution has several stages to it, with an initial concentric circle pattern that was previously noted in [2] and is due to an interaction between the unstable plane wave and the unstable localized bump. At a slower time scale is the local stability of the hexagonal units' peaks, and that later gives way to the even slower scale sorting done by through the hexagonal unit's tails. The only observed stable steady state arrangement in this regime are the hexagonal pattern displayed in the bottom right of figure 17 and other highly symmetric patterns on periodic domains with periods too small to fit a hexagonal pattern. The stability of the hexagonal pattern was confirmed by numerically calculating the linear stability, which shows it to have only real valued, negative eigenvalues. However, when two separate regions with a hexagonal pattern but opposite signs are placed next to each other the two hexagonal regions repulse each other. This repulsion, combined with the hexagonal pattern's own robustness allows for structural oscillations, involving spontaneous structure creation and destruction as seen in figure 18. That the domain is periodic ensures that such oscillations can persist.

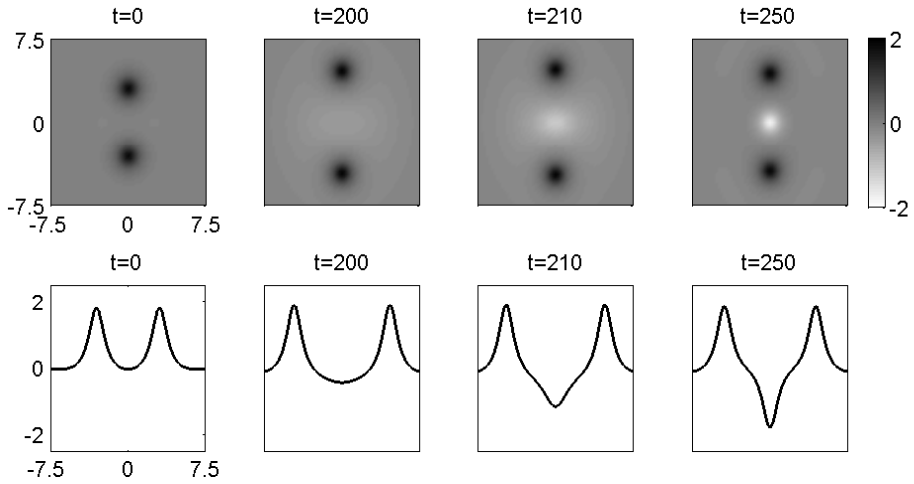

Figure 12: Shown above is the evolution of two LS of the same sign a moderate distance apart under the same parameter regime as figure 11. Notice that the LS initially repel each other, only to then have a LS of opposite sign appear in between them. Seen in the cross section of the plot the negative tails of the two LS create dip (center left) which is an unstable mode of the zero plane wave, leading to the creation of a negative LS.

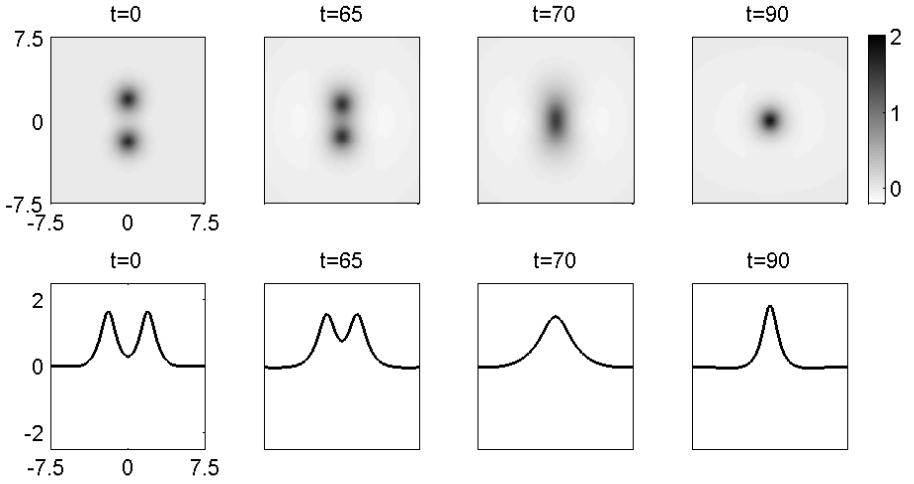

Figure 13: Shown above is the same setup as figure 12, with two LS of the same sign, except that these LS are closer together. For this spacing these LS collide and merge into a single LS. A key difference between this spacing and the one in figure 12 is that, as seen in the cross section, the tails between the two LS are positive, creating a situation much like the non monotonic tail case in figure 10.

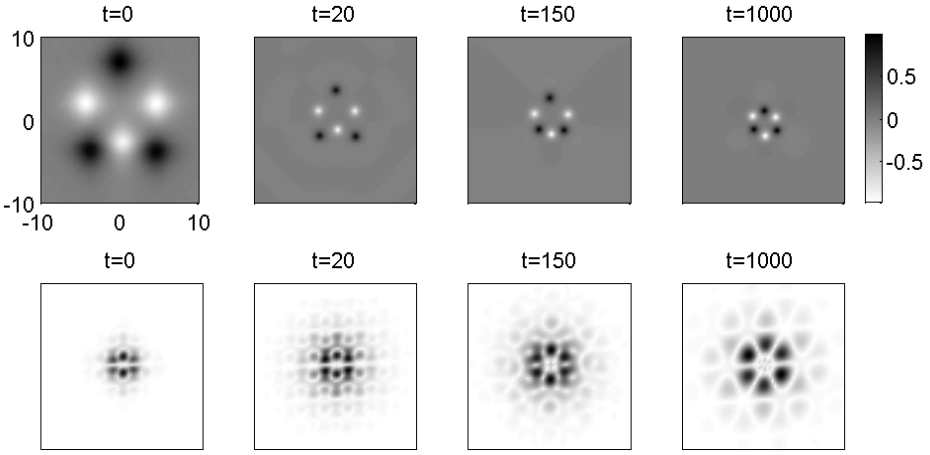

Figure 14: As a result of the optimal spacing seen in figure 11 it is possible for LS to arrange themselves spatially as seen above with six LS of alternating sign. The bottom evolution displays the modulus of the Fourier transform of the transform.

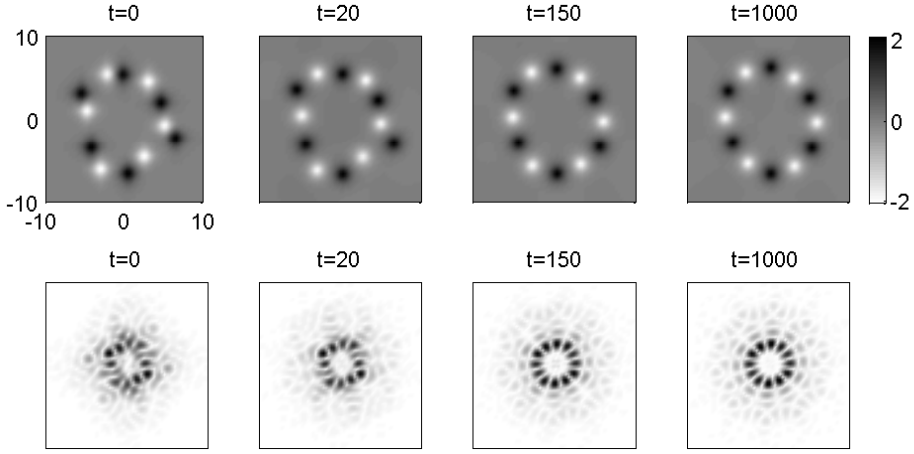

Figure 15: Much as in figure 14 this evolution displays the creation of spatial pattern composed of LS of alternating sign (top) and the modulus of the corresponding Fourier Transforms (bottom).

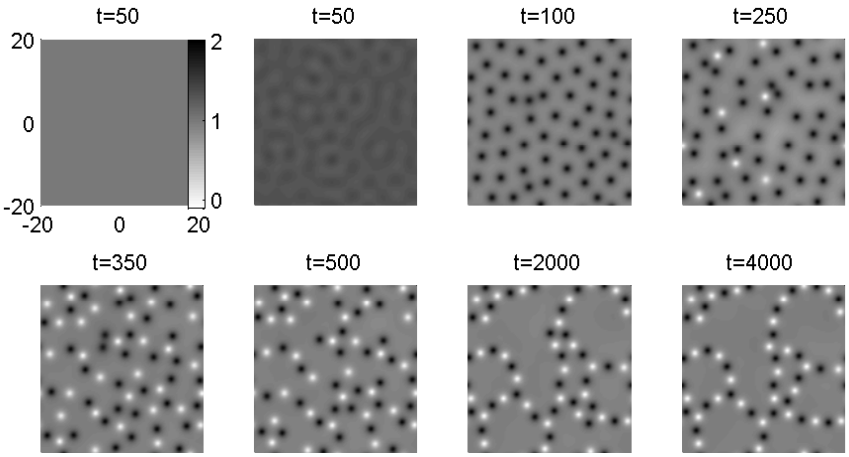

Figure 16: Starting from an unstable, positive amplitude plane wave with noise we see the creation of complicated LS structures in a several stage process in the same parameter regime as figures 11 to 15. Initially the instability of the positive plane wave drives the creation of solely positive LS. Only then can LS-LS interactions, which occur at a slower rate than the plane wave instability, become the dominant behavior. LS merging, as seen in figure 13 is a fast interaction, which is then followed by the slower tail mitigated creation of negative LS. Once positive and negative LS have formed the LS begin arranging themselves into a combination of stable, rings, lines and grids.

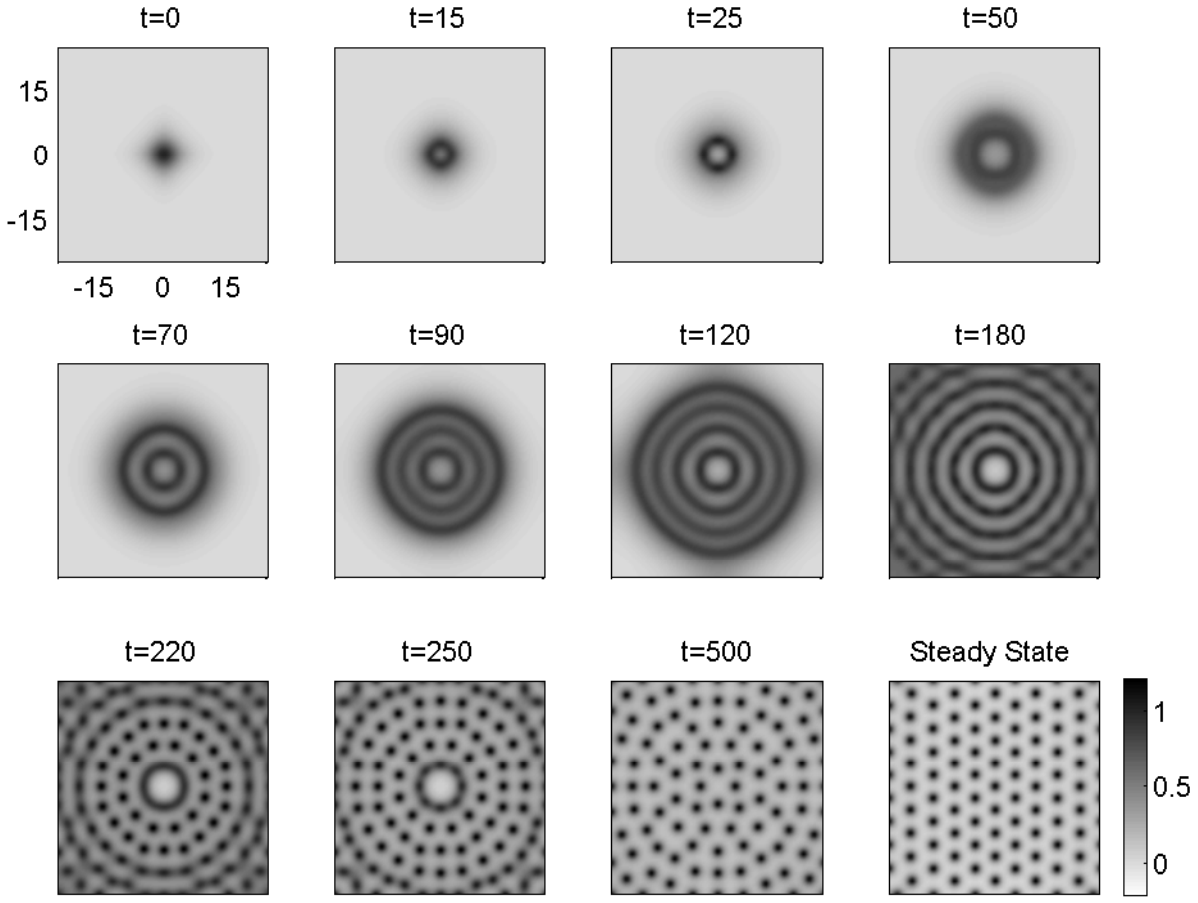

Figure 17: Shown above is the evolution of a hexagonal type pattern from an initial lump on top of the unstable 0 plane wave for parameters, $\gamma = .1$, $\omega = .5$ and $\sigma = .472$. The bottom right plot displays a stable, steady-state solution for this parameter regime that displays the characteristic hexagonal pattern so often seen in Swift-Hohenberg equations.

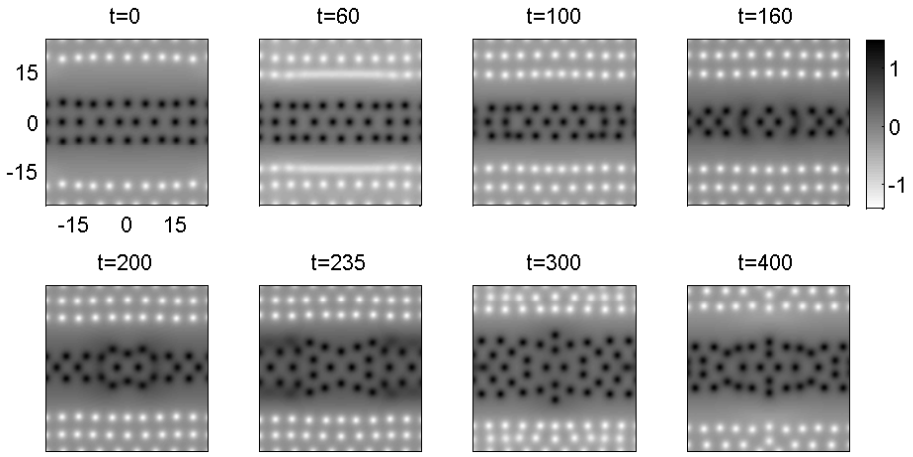

Figure 18: Under the same parameter regime as figure 17 two hexagonal regions of opposite sign can be observed to pulsate. As can be seen in the figure the hexagonal regions expand through pushing out a wave that leaves hexagonal units in its wake, and similar they shrink through hexagonal units coalescing

5 3D Structures

Ultimately the physical structure of an OPO crystal is 3D, and thus full 3D modeling is the most practically important. While it will turn out that many 2D structures are unstable in 3D, the intuition gained from the 2D behavior has analogous application in 3D.

5.1 LS in 3D

The LS found in 2D, when directly extended to 3D, is unstable. However, much as the sech was unstable in 2D, the 2D LS has instability that itself is a localized steady-state stable solution in 3D that is radially symmetric. Figure 19 displays a 3D LS. Notice that the amplitudes of the LS increase according to the number of additional spatial dimensions, which makes since as nonlinearity is used to balance the diffusive terms, which have strong radial effects for increasing spatial dimensions. The 3D LS maintains the same large basin of attraction that the 2D had. Figure 20 displays the evolution of a set of LS from an constant wave with noise in the interior. In the same way that the 2D LS with strictly positive tails displayed purely attractive LS-LS interactions these 3D LS also are attracted to one another.

Similarly 3D LS analogous to the Non monotonic tail 2D LS and sphere packing LS in the hexagonal parameter regime have been found and display behavior analogous to their 2D counterparts.

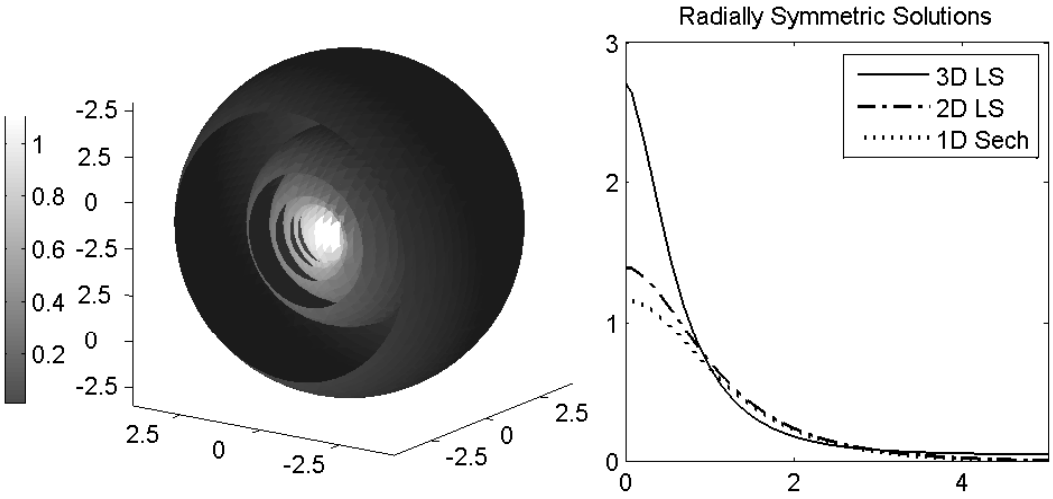

Figure 19: Shown left is an isosurface of a 3D radially symmetric LS for parameters, $\gamma = .03$, $\sigma = \omega = .5$. The plot on the right displays the radial components of the 1D sech, and the 2D and 3D LS for this parameter regime. Notice that in order for nonlinearity to balance the increasing diffusive terms associated with higher dimensions the magnitude of the LS also increases with the number of dimensions. Aside from the large magnitude of the 3D LS the shape and tail structure of the LS remains fairly similar to the 2D LS and 1D sech.

6 Conclusions

We have derived an order parameter equation for the non-degenerate optical parametric oscillator near its resonance detuning limit and have used that OPE, albeit in its degenerate limit, to analyze the behavior of the OPO near its resonance detuning limit. A broad class of localized solutions were found that have two different tail structures, allowing for two very different LS-LS interactions. In particular, a class of LS was found that can assemble stable and nontrivial spatial structures, including rings, lines and grids. Additionally the stability of these LS was confirmed utilizing the Floquet-Fourier Hill method to calculate linear stability. Additionally the stability of 1D solutions found previously was reviewed with the conclusion that the solutions with sharp fronts and large shelfs, tanh and sn remained stable, while cn, dn and sech are fundamentally unstable in 2D. The dynamics of solutions with tanh transitions was also investigated. As with many Swift-Hohenberg type equations, a regime in which hexagonal patterns dominated was also found. In particular the hexagonal patterns were found to be able to have structural oscillations. Finally the stability of the 2D LS was examined in 3D, where it was found that while the 2D LS was unstable, there existed an analogous 3D LS, which demonstrated similar LS-LS interactions.

References

[1] S. E. Hewitt and J. N. Kutz. *Dynamics of the optical parametric oscillator near resonance detuning,* J. SIAM J. Apl. Dynamical Systems. Vol. 4, No. 808-831 (2005).

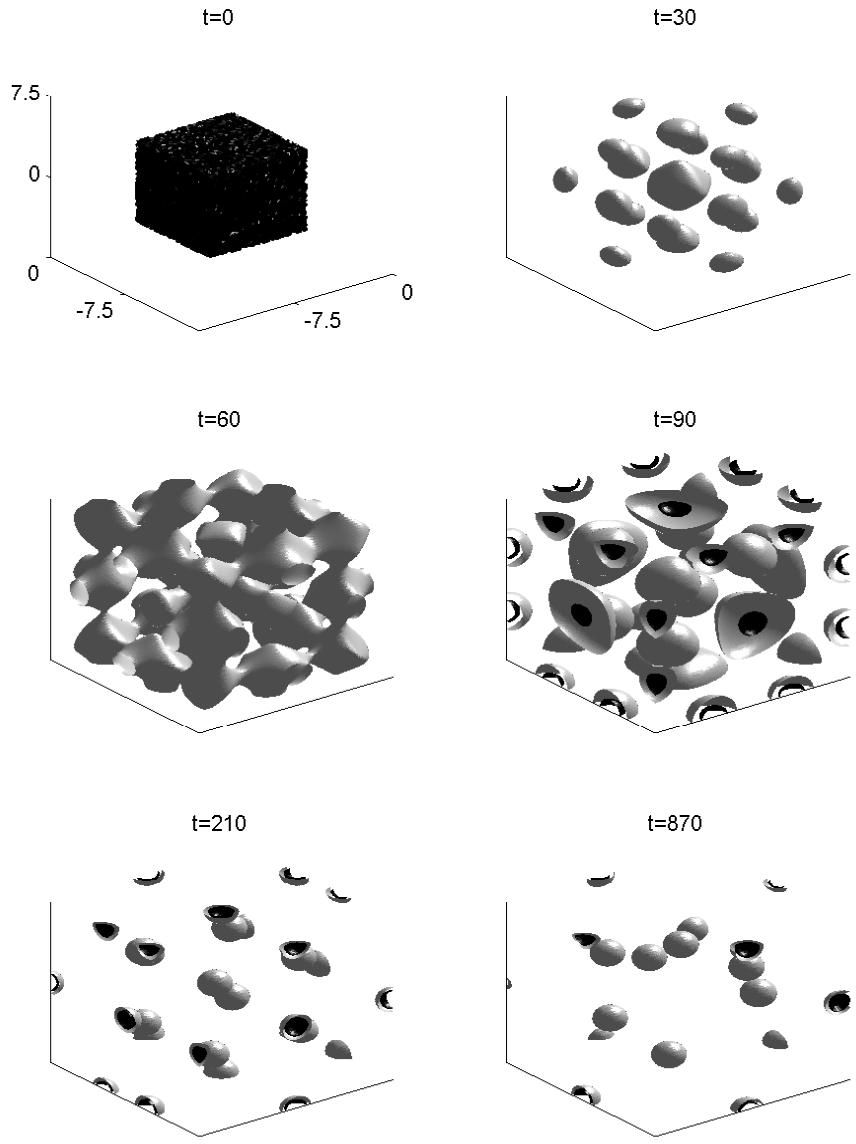

Figure 20: Under the same parameter regime as figure 19 and using isosurface values of .6 and 1 we see the formation of 3D LS from an unstable plane wave with noise. Notice that the LS-LS interactions present, with LS attracting and combining near the end is reminiscent of the 2D LS behavior in the monotonic tail case.

[2] B. Osting, S. E. Hewitt and J. N. Kutz. *Stability and dynamics of transverse field structures in the optical paramtreic oscillator near resonance signal detuning,* J. Physics B. **13**, 3461-3475 (2005).

[3] S. Longhi, A. Geraci. *Swift-Hohenberg equation for optical parametric oscillators,* Phys. Rev. A 54, 4581 - 4584 (1996).

[4] A. Kassam and L. N. Trefethen. *Fourth-order time-stepping for stiff PDEs,* SIAM J. Sci. Comput. **39**, 1214-1233 (2005).

[5] J. N. Kutz. *Pulse Propagation in Nonlinear Optical Fibers using Phase-Sensitive Amplifiers,* Ph.D. Thesis (1994).

[6] S. Trillo, M. Haelterman and A. Sheppard. *Excitation and bistability of self-trapped signal beams in optical parametric oscillators,* Opt. Lett. **23** 1514 (1998).

[7] K. Staliunasa and V. J. Sanchez-Morcillo. *Transverse patterns in nonlinear optical resonators,* Springer, NY. 2003

[8] B. Deconinck and J. N. Kutz. *Computing spectra of linear operators using Hill's method,* Journal of Computational Physics 219 (2006) 296-321.